OPEN

Robust antiferromagnetism preventing superconductivity in pressurized $(Ba_{0.61}K_{0.39})Mn_2Bi_2$

Dachun Gu[1], Xia Dai[1], Congcong Le[1], Liling Sun[1,2], Qi Wu[1], Bayrammurad Saparov[3], Jing Guo[1], Peiwen Gao[1], Shan Zhang[1], Yazhou Zhou[1], Chao Zhang[1], Shifeng Jin[1], Lun Xiong[4], Rui Li[4], Yanchun Li[4], Xiaodong Li[4], Jing Liu[4], Athena S. Sefat[3], Jiangping Hu[1,2] & Zhongxian Zhao[1,2]

[1]Institute of Physics and Beijing National Laboratory for Condensed Matter Physics, Chinese Academy of Sciences, Beijing 100190, China, [2]Collaborative Innovation Center of Quantum Matter, Beijing, 100190, China, [3]Materials Science and Technology Division, Oak Ridge National Laboratory, Oak Ridge, TN 73831-6056, USA, [4]Institute of High Energy Physics, Chinese Academy of Sciences, Beijing 100049, China.

$BaMn_2Bi_2$ possesses an iso-structure of iron pnictide superconductors and similar antiferromagnetic (AFM) ground state to that of cuprates, therefore, it receives much more attention on its properties and is expected to be the parent compound of a new family of superconductors. When doped with potassium (K), $BaMn_2Bi_2$ undergoes a transition from an AFM insulator to an AFM metal. Consequently, it is of great interest to suppress the AFM order in the K-doped $BaMn_2Bi_2$ with the aim of exploring the potential superconductivity. Here, we report that external pressure up to 35.6 GPa cannot suppress the AFM order in the K-doped $BaMn_2Bi_2$ to develop superconductivity in the temperature range of 300 K–1.5 K, but induces a tetragonal (T) to an orthorhombic (OR) phase transition at ~20 GPa. Theoretical calculations for the T and OR phases, on basis of our high-pressure XRD data, indicate that the AFM order is robust in the pressurized $Ba_{0.61}K_{0.39}Mn_2Bi_2$. Both of our experimental and theoretical results suggest that the robust AFM order essentially prevents the emergence of superconductivity.

Superconductivity in unconventional high-temperature (high-Tc) superconductors is related to an antiferromagnetic (AFM) ground state in an undoped layered 'parent' compound[1–5]. Therefore, the layered AFM compounds with higher Neel temperature (T_N) are believed to be good candidates for the parent compounds of new high-Tc superconductors[6]. The Mn-pnicitides of Mn-1111 and Mn-122 compounds, such as $LaMnPO$[7–9], $BaMn_2P_2$[10–12], $BaMn_2As_2$[13–22] and $BaMn_2Bi_2$[23–25], are such kinds of compounds, having AFM ground state similar to the parent compounds of cuprates[26] and the same crystal structure as Fe-pnictides[2,3]. For such similarities, it is reasonably expected that the $BaMn_2Bi_2$ might be a parent compound of Mn-based superconductors.

Previous studies demonstrated that the AFM order in the parent compounds of cuprates and FeAs-based superconductors can be efficiently suppressed by either external pressure or chemical doping, driving the samples into a superconducting state[2,4,27–40]. Neutron studies show that $BaMn_2Bi_2$ has an alternative magnetic structure from the parent compounds of cuprates and FeAs-122 superconductors, adopting G-type AFM with $T_N = 387$ K in the tetragonal phase[24]. Doping potassium (K) for Ba sites has turned the sample from an insulating/semiconducting state to a metallic state[23], but it has no significant effect on its AFM order. In this work, we perform high-pressure investigations on the $Ba_{0.61}K_{0.39}Mn_2Bi_2$ by in-situ high pressure electrical transport and X-ray diffraction (XRD) measurements in a diamond anvil cell (DAC). We find no evidence of superconductivity in the pressurized $Ba_{0.61}K_{0.39}Mn_2Bi_2$ up to 35.6 GPa, however, a pressure-induced tetragonal (T)-to-orthorhombic (OR) phase transition is observed. Our in-situ high pressure ac susceptibility measurements and theoretical calculations reveal that the $Ba_{0.61}K_{0.39}Mn_2Bi_2$ has robust antiferromagnetism in both of the T phase and OR phase, and is a strong Hund's AFM metal with a hybridization between localized spin electrons and itinerant electrons.

Results

Figure 1(a) and 1(b) show temperature (T) dependent of resistance (R) of the $Ba_{0.61}K_{0.39}Mn_2Bi_2$ under pressure up 35.6 GPa. It is found that the R-T curves are pressure dependent, i.e. the R-T curve moves up with increasing

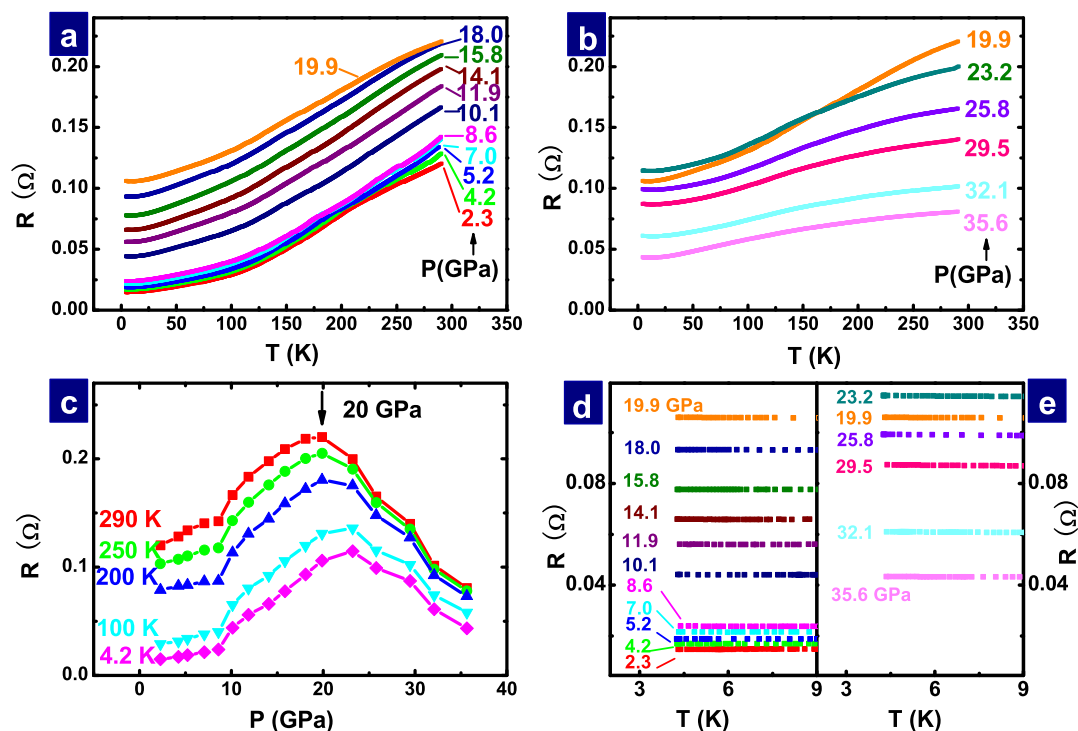Figure 1 | Electrical resistance as a function of temperature and pressure for $Ba_{0.61}K_{0.39}Mn_2Bi_2$. (a) and (b) Temperature dependent resistance of $Ba_{0.61}K_{0.39}Mn_2Bi_2$ at different pressures. (c) Pressure dependence of resistance measured at different temperatures, displaying a dome-like feature centered at ~20–23 GPa. (d) and (e) Blown-up R-T curves at different pressures, showing no evidence of superconductivity.

pressure up to 19.9 GPa, while it changes its trend with further increasing pressure ranging from 19.9 to 35.6 GPa. Plot of pressure dependence of resistance measured at different temperatures illustrates this conspicuous feature (Fig. 1c). This feature may be associated with a first-order structure phase transition. Zooming in the R-T curves for lower temperature range, we found no sign of pressure-induced superconductivity down to 1.5 K under pressure up to 35.6 GPa (Fig. 1d and 1e). To confirm the experimental results obtained in $Ba_{0.61}K_{0.39}Mn_2Bi_2$, we loaded the sample with the actual composition of $Ba_{0.68}K_{0.32}Mn_2Bi_2$ from Sefat's Group into a DAC in a glove-box and performed experiments in the same manner. We observed the same high pressure behavior as found in $Ba_{0.61}K_{0.39}Mn_2Bi_2$.

Structure is crucial in tailoring the superconductivity. At ambient pressure, $BaMn_2Bi_2$ adopts a body-centered $ThCr_2Si_2$ tetragonal structure in the space group $I4/mmm$. Hole-doping via substitution of Ba with K in the form of $Ba_{1-x}K_xMn_2Bi_2$ does not alter its crystal structure[23]. While, applying pressure on the $Ba_{0.61}K_{0.39}Mn_2Bi_2$ in this study found a T-OR phase transition at 19.8 GPa, as shown in Fig. 2(a), very similar to the case seen in the pressurized $LaMnPO$[8]. The OR phase in $Ba_{0.61}K_{0.39}Mn_2Bi_2$ persists up to 28.8 GPa. The evolutions of its lattice parameters and volume with pressure in the two phases are displayed in Fig. 2(b) and 2(c). The pressure induced T-OR phase transition determined by high-pressure XRD measurements is consistent with our resistance data. As shown in Fig. 1c, pressure dependence of resistance displays a dome-like feature. The resistance increases with pressure, reaches a maximum at ~20 GPa and then decreases with further increasing pressure. Notably, the change in resistance against pressure follows the similar trend at different temperatures down to 4 K, indicating that either the room-temperature T phase or the room-temperature OR phase can be maintained down to 4 K.

Figure 2(d) and 2(e) present XRD patterns of the pressurized sample and corresponding Rietveld refinement results. It is seen that the XRD pattern obtained at 1.7 GPa can be well refined as the T

phase in the $I4/mmm$ space group, yielding the reliability factor of R_p = 4.65% and weighted factor of R_{wp} = 6.18%, respectively, as well as the fitting goodness χ^2 = 1.242. The refinement of the XRD data collected at 19.8 GPa is in good agreement with OR phase in the $Fmmm$ space group; the R_p = 4.77%, R_{wp} = 5.84% and χ^2 = 1.421, respectively. The obtained R values in the two phases are comparable with the refinement for the ambient-pressure data of the same material[23]. Figure 2(f) shows the X-ray diffraction images for the $Ba_{0.61}K_{0.39}Mn_2Bi_2$ at different pressures. It is seen that the quality of the crystallinity is getting worse with increasing pressure. At 28.8 GPa, a halo-like ring is observed, together with corresponding broadening XRD pattern suggesting that part of the OR phase has transformed to an amorphous-like phase.

To trace the evolution of T_N of $Ba_{0.61}K_{0.39}Mn_2Bi_2$ with pressure, we performed high-pressure alternating current (ac) susceptibility measurements for the sample in a house-built refrigerator[41]. Although there is no experimental data that confirm AFM ground state of $Ba_{0.61}K_{0.39}Mn_2Bi_2$ and allow to evaluate T_N at ambient pressure, magnetization results for $Ba_{1-x}K_xMn_2As_2$ at lower doping level ($x \leq 0.1$) show the existence of the AFM ground state above 400 K[13,17,21]. Moreover, the similar magnetically anisotropic phenomenon is observed in both of $Ba_{0.9}K_{0.1}Mn_2Bi_2$ and $Ba_{0.68}K_{0.32}Mn_2Bi_2$[23]. Together with the result of the same temperature dependence of resistance in pressurized $Ba_{0.61}K_{0.39}Mn_2As_2$ and $Ba_{0.68}K_{0.32}Mn_2Bi_2$, we argue that the uncompressed $Ba_{0.61}K_{0.39}Mn_2Bi_2$ is in the AFM state below 300 K. In our ac susceptibility measurements, the direction of the applied magnet field is perpendicular to the ab plane of the single crystal. As shown in Fig. 3, the temperature dependence of the ac susceptibility is featureless at 3.1 GPa, except for a broad hump in higher temperature range. Further investigation indicates that this broad hump is not from the sample intrinsically, but originated from the trace impurity in the supporting plate of diamond anvils. The χ as a function of temperature at 3.1 GPa is consistent with the ambient-pressure result[23]. With increasing pressure up to 20.2 GPa, the temperature
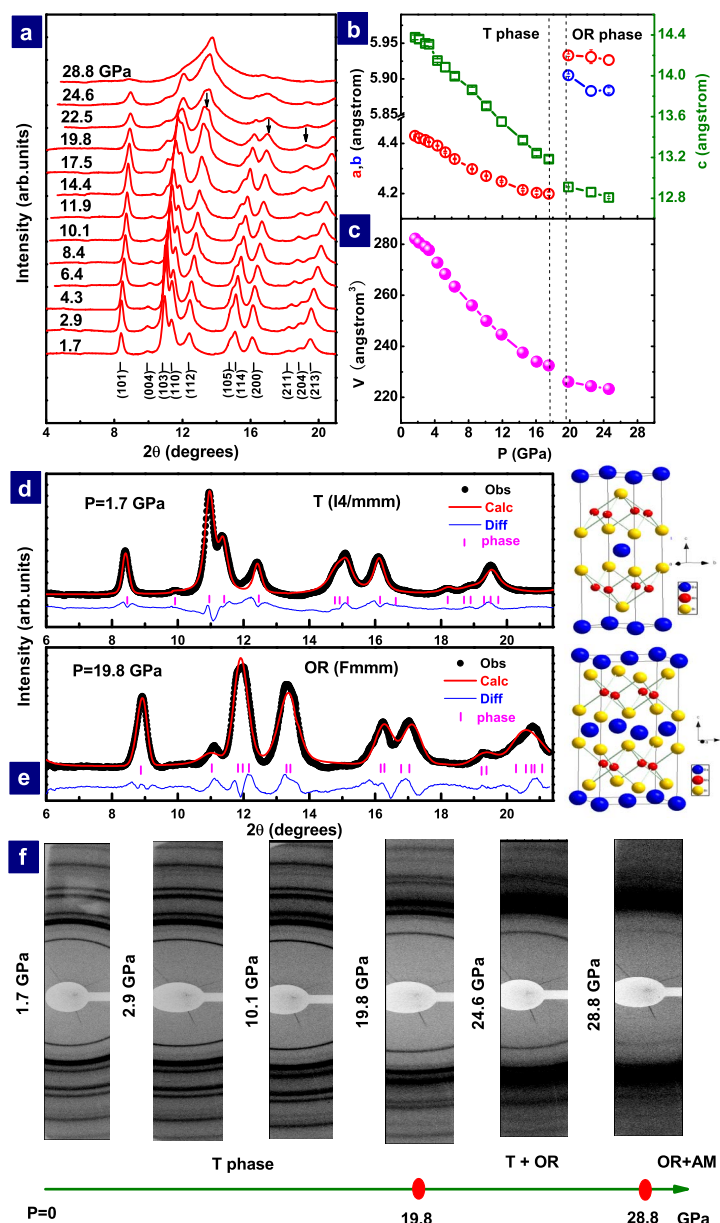
Figure 2 | X-ray diffraction patterns and Rietveld refinements results of $Ba_{0.61}K_{0.39}Mn_2Bi_2$ at different pressures and its lattice parameter and volume as a function of pressure. (a) Representative XRD patterns for $Ba_{0.61}K_{0.39}Mn_2Bi_2$ at various pressures. (b) Pressure dependence of lattice constant a (red circle, $a = b$ in the T phase), b (blue circle) and c (green square). (c) Volume as a function of pressure in the tetragonal (T) and orthorhombic (OR) phases. (d) and (e) Rietveld refinement results of the X-ray diffraction patterns in the tetragonal (T) phase ($I4/mmm$) at 1.7 GPa and the orthorhombic (OR) phase ($Fmmm$) 19.8 GPa, together with the corresponding crystal structures shown on the right. (f) Representative X-ray diffraction images at different pressures, showing structure evolution with pressure.

dependence of real part (χ) of the ac susceptibility remains unchanged. This demonstrates that the T_N of the pressurized $Ba_{0.61}K_{0.39}Mn_2Bi_2$ is still higher than 300 K, otherwise it should be detected by our instrument, as done in pressurized $LaMnPO$[9].

Discussion

It is known that, with pressure-induced volume shrinking, the band structure and density-of-states (DOS) may change correspondingly. To identify whether the pressure may induce a significant change in electronic structure, we carried out theoretical calculations on basis of our high-pressure XRD data for the T and OR phases of $Ba_{1-x}K_xMn_2Bi_2$. Our calculation results are summarized in Fig. 4. We find that the ground state of the pressurized $Ba_{0.61}K_{0.39}Mn_2Bi_2$ is a robust G-type AFM metal in the T phase with an ordered magnetic moment $\sim$3.4 μ_B/Mn aligned parallel to the c axis. The band
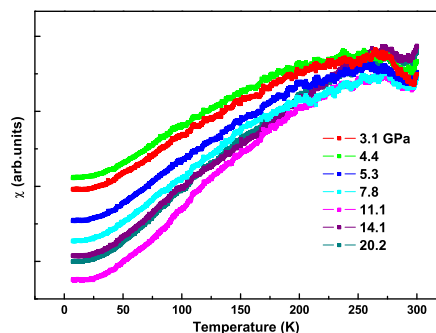

Figure 3 | Raw data of the temperature dependence of ac susceptibility of the $Ba_{0.61}K_{0.39}Mn_2Bi_2$ at different pressures.
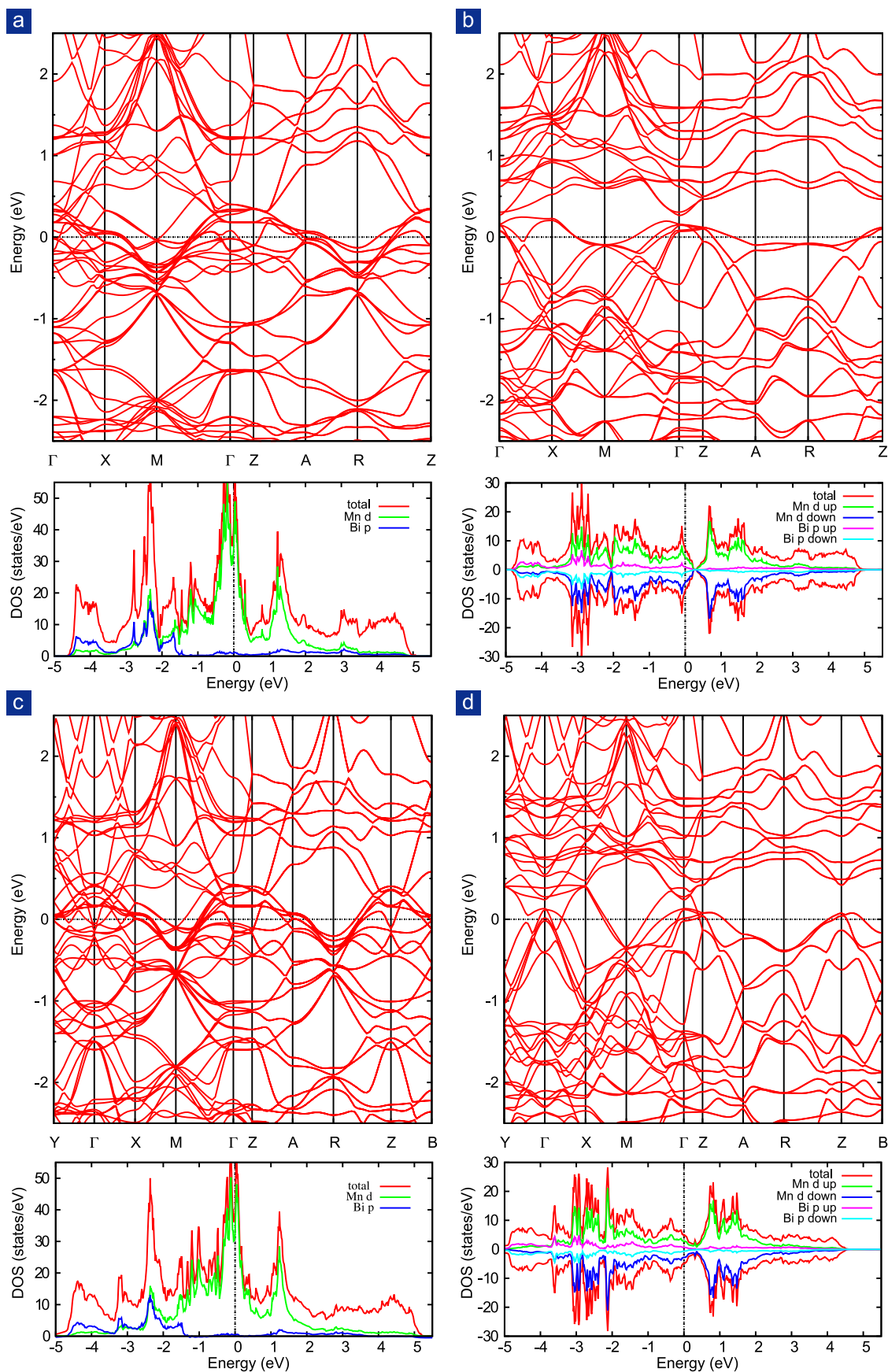
Figure 4 | Band structures and density-of-states at 17.49 GPa and 24.6 GPa. (a) and (b) Band structures and density-of-states for the tetragonal phase of $Ba_{0.61}K_{0.39}Mn_2Bi_2$ at 17.49 GPa in the paramagnetic and antiferromagnetic states, respectively. (c) and (d) Band structures and density-of-states for the orthorhombic phase of $Ba_{0.61}K_{0.39}Mn_2Bi_2$ at 24.6 GPa in the paramagnetic and antiferromagnetic states, respectively.

structure and DOS of the $Ba_{0.61}K_{0.39}Mn_2Bi_2$ in the paramagnetic (PM) and AFM states at 17.49 GPa are shown in Fig. 4(a) and Fig. 4(b), respectively. Both states are metallic. In the AFM state, the total energy per unit cell is lower than that in the PM state (Supplementary Information), indicating that the AFM state is the ground state. In the PM state, the $3d$ states of Mn dominate near Fermi level as shown in Fig. 4(a). However, in the AFM state, there is large weight redistribution for the $3d$ states of Mn. The $3d$ electron density has large concentration from -3 eV to -2 eV and from 0.5 eV to 2 eV, which indicate the large energy splitting caused by the AFM ordering, consistent with the large local spin moment formed through strong Hund's coupling[42]. In the OR phase, the band structure and DOS at 24.6 GPa in both PM and AFM states of the OR phase are almost unchanged (Fig. 4(c) and Fig. 4(d)). The ground state is still a G-type AFM state with a magnetic moment of ~3.3 μ_B/Mn. However, the direction of magnetic moment is parallel to the a-axis. Comparing with the band structure and DOS at 17.49 GPa, our results indicate that K-doped $BaMn_2Bi_2$ seems completely insensitive to pressure. The theoretical calculations are in good agreement with our high-pressure ac susceptibility results (Fig. 3).

Comparing with the evolution of AFM order with pressure in Fe-based pnictides[43,44] and chalcogenides[45,46] whose AFM order can be destroyed at modest pressure below ~10 GPa, the AFM order in the K-doped $BaMn_2Bi_2$ exhibits insensitive to pressure. These results demonstrates that the Mn's d^5 electrons in the sample investigated are much more localized than Fe's d^6 electrons in the Fe-based pnictides and Fe-based chalcogenides, which leads to the K-doped $BaMn_2Bi_2$ belongs to a strong Hund's AFM metal with a hybridization between localized spin electrons and itinerant electrons.

Our previous high studies on LaMnPO showed that the similar pressure as applied on the K-doped $BaMn_2Bi_2$ is sufficient to completely destroy the AFM order[9]. The different responses to pressure between these two Mn-containing compounds may be associated to the different anion radii between these two kinds of pnictides. The radius of P anion in LaMnPO is considerably smaller than that of Bi anion in $BaMn_2Bi_2$, which leads to the overlap and interaction between the d-orbital of Mn and the p-orbital of Bi much less than those between the d-orbital of Mn and the p-orbital of P in LaMnPO. As we know that the d-p interaction is the key to mediate the AFM order, as a result, the AFM order in $BaMn_2Bi_2$ is much more robust than LaMnPO in the same pressure regime.

In conclusion, in-$situ$ high-pressure measurements of resistance, ac susceptibility and XRD as well as theoretical calculations find that the AFM order in $Ba_{0.61}K_{0.39}Mn_2Bi_2$ is robust under external pressure. No evidence for superconductivity is found under pressure up to 35.6 GPa, however, a pressure-induced structural transition from T phase to OR phase is observed at ~20 GPa. Theoretical calculations demonstrate that the values of magnetic moment on Mn in the T phase and OR phase are nearly identical, suggesting that the K-doped $BaMn_2Bi_2$ is a strong Hund's AFM metal with a hybridization of localized spin electrons and itinerant electrons. The robust AFM order in $Ba_{0.61}K_{0.39}Mn_2Bi_2$ essentially prevents the emergence of superconductivity.

Methods

High quality single crystals with nominal composition $Ba_{0.4}K_{0.6}Mn_2Bi_2$ were synthesized by the similar method as described in Ref. 23. High-pressure resistance measurements using the standard four-probe method were performed in a DAC made from Be-Cu alloy in a house-built refrigerator with closed cycle refrigeration[41]. Diamond anvils of 500 μm and 300 μm flats were used for this study. NaCl powders were employed as pressure medium for the high-pressure resistance measurements. High-pressure ac susceptibility measurements were conducted using home-made coils that were wound around a diamond anvil[41,47]. The nonmagnetic rhenium gasket with 200 μm and 100 μm diameter sample holes was used for different runs of high-pressure resistance and magnetic measurements. Structural information under pressure was obtained through the angle-dispersive powder XRD experiments, performed at beamline 4W2 at the Beijing Synchrotron Radiation Facility (BSRF). Diamonds with low birefringence were selected for the high-pressure XRD experiments. A monochromatic X-ray beam with a wavelength of 0.6199 Å was adopted for all measurements. To keep the sample in a quasi-hydrostatic pressure environment, silicon oil was used for the XRD measurements. Pressure was determined by ruby fluorescence method[48]. Since the sample is air sensitive, the samples either for high-pressure resistance or XRD measurements were loaded into the DAC in a glove-box.

Our calculations were performed using density functional theory (DFT) as implemented in the Vienna ab initio simulation package (VASP) code[49]. The Perdew-Burke-Ernzerhof (PBE) exchange-correlation functional[50] and the projector-augmented-wave (PAW) approach[51] are used. Throughout the work, the cutoff energy is set to be 400 eV. The positions of all the atoms are fully relaxed during the geometry optimizations with forces minimized to less than 0.01 eV/Å. On the basis of the equilibrium structure, 20 k points are used to compute the band structure. We have also performed GGA + U calculations, where U is the onset coulomb repulsive energy of Mn. With a modest U value (5 eV), we find that the result reported in the following for both band structures and magnetisms are not qualitatively modified.

1. Cava, R. J., van Dover, R. B., Batlogg, B. & Rietman, E. A. Bulk superconductivity at 91 K in single-phase oxygen-deficient perovskite $Ba_2YCu_3O_{9-\delta}$. *Phys. Rev. Lett.* **58**, 408 (1987).
2. Kamihara, Y., Watanabe, T., Hirano, M. & Hosono, H. Iron-Based Layered Superconductor La[$O_{1-x}F_x$]FeAs (x = 0.05–0.12) with Tc = 26 K. *J. Am. Chem. Soc.* **130**, 3296 (2008).
3. Rotter, M., Tegel, M. & Johrendt, D. Superconductivity at 38 K in the iron arsenide ($Ba_{1-x}K_x$)Fe_2As_2. *Phys. Rev. Lett.* **101**, 107006 (2008).
4. Torikachvili, M. S., Bud'ko, S. L., Ni, N. & Canfield, P. C. Pressure Induced Superconductivity in $CaFe_2As_2$. *Phys. Rev. Lett.* **101**, 057006 (2008).
5. Jiang, S. et al. Superconductivity up to 30 K in the vicinity of the quantum critical point in BaFe$2(As$_{1-x}P_x$)$_2$. *J. Phys.: Condens. Matter* **21**, 382203 (2009).
6. Anderson, P. W. The Resonating Valence Bond State in La_2CuO_4 and Superconductivity. *Science* **235**, 1196 (1987).
7. Simonson, J. W. et al. Gap states in insulating $LaMnPO_{1-x}F_x$ (x = 0–0.3). *Phys. Rev. B* **84**, 165129 (2011).
8. Simonson, J. W. et al. From antiferromagnetic insulator to correlated metal in pressurized and doped LaMnPO. *Proc. Natl. Acad. Sci. U.S.A.* **109**, E1815–E1819 (2012).
9. Guo, J. et al. Observation of antiferromagnetic order collapse in the pressurized insulator LaMnPO. *Sci. Rep.* **3**, 2555 (2013).
10. Kamiya, T., Yanagi, H., Watanabe, T., Hirano, M. & Hosono, H. Electronic structures of MnP-based crystals: $LaMnOP$, $BaMn_2P_2$, and KMnP. *Mater. Sci. Eng. B* **173**, 239 (2010).
11. Brock, S. L., Greedan, J. E. & Kauzlarich, S. M. Resistivity and Magnetism of AMn_2P_2 (A = Sr, Ba): The Effect of Structure Type on Physical Properties. *J. Solid State Chem.* **113**, 303 (1994).
12. Hoffmann, R. & Zheng, C. Making and breaking bonds in the solid state: the thorium chromium silicide ($ThCr_2Si_2$) structure. *J. Phys. Chem.* **89**, 20 (1985).
13. Singh, Y., Ellern, A. & Johnston, D. C. Magnetic, transport, and thermal properties of single crystals of the layered arsenide $BaMn_2As_2$. *Phys. Rev. B* **79**, 094519 (2009).
14. Singh, Y. et al. Magnetic order in $BaMn_2As_2$ from neutron diffraction measurements. *Phys. Rev. B* **80**, 100403(R) (2009).
15. An, J., Sefat, A. S., Singh, D. J. & Du, M. H. Electronic structure and magnetism in $BaMn_2As_2$ and $BaMn_2Sb_2$. *Phys. Rev. B* **79**, 075120 (2009).
16. Satya, A. T. et al. Pressure-induced metallization of $BaMn_2As_2$. *Phys. Rev. B* **84**, 180515(R) (2011).
17. Pandey, A. et al. $Ba_{1-x}K_xMn_2As_2$: An antiferromagnetic local-moment metal. *Phys. Rev. Lett.* **108**, 087005 (2012).
18. Lamsal, J. et al. Persistence of local-moment antiferromagnetic order in $Ba_{1-x}K_xMn_2As_2$. *Phys. Rev. B* **87**, 144418 (2013).
19. Pandey, A. et al. Coexistence of half-metallic itinerant ferromagnetism with local-moment antiferromagnetism in $Ba_{0.60}K_{0.40}Mn_2As_2$. *Phys. Rev. Lett.* **111**, 047001 (2013).
20. Glasbrenner, J. K. & Mazin, I. I. First-principles evidence of Mn moment canting in hole-doped $Ba_{1-2x}K_{2x}Mn_2As_2$. *Phys. Rev. B* **89**, 060403(R) (2014).
21. Bao, J. K. et al. Weakly ferromagnetic metallic state in heavily doped $Ba_{1-x}K_xMn_2As_2$. *Phys. Rev. B* **85**, 144523 (2012).
22. Antal, A. et al. Optical properties of the iron-pnictide analog $BaMn_2As_2$. *Phys. Rev. B* **86**, 014506 (2012).
23. Saparov, B. & Sefat, A. S. Crystals, magnetic and electronic properties of a new $ThCr_2Si_2$-type $BaMn_2Bi_2$ and K-doped compositions. *J. Solid State Chem.* **204**, 32 (2013).
24. Calder, S. et al. Magnetic structure and spin excitations in $BaMn_2Bi_2$. *Phys. Rev. B* **89**, 064417 (2014).
25. Wang, K. F. & Petrovic, C. Large thermopower in the antiferromagnetic semiconductor $BaMn_2Bi_2$. *Appl. Phys. Lett.* **103**, 192104 (2013).
26. Armitage, N. P., Fournier, P. & Greene, R. L. Progress and perspectives on electron-doped cuprates. *Rev. Mod. Phys.* **82**, 2421 (2010).
27. Takahashi, H. et al. Superconductivity at 43 K in an iron-based layered compound $LaO_{1-x}F_xFeAs$. *Nature* **453**, 376 (2008).
28. Ren, Z. A. et al. Superconductivity at 55 K in iron-based F-doped layered quaternary compound $Sm[O_{1-x}F_x]FeAs$. *Chin. Phys. Lett.* **25**, 2215 (2008).
29. Alireza, P. L. et al. Superconductivity up to 29 K in $SrFe_2As_2$ and $BaFe_2As_2$ at high pressures. *J. Phys.: Condens. Matter* **21**, 012208 (2009).

30. Park, T. *et al*. Pressure-induced superconductivity in CaFe$_2$As$_2$. *J. Phys.: Condens. Matter* **20**, 322204 (2008).

31. Zheng, Y., Wang, Y., Lv, B., Chu, C. W. & Lortz, R. Thermodynamic evidence for pressure-induced bulk superconductivity in the Fe–As pnictide superconductor CaFe$_2$As$_2$. *New J. Phys.* **14**, 053034 (2012).

32. Iimura, S. *et al*. Two-dome structure in electron-doped iron arsenide superconductors. *Nat. Comm.* **3**, 943 (2012).

33. Terashima, T. *et al*. EuFe$_2$As$_2$ under High Pressure: An antiferromagnetic bulk superconductor. *J. Phys. Soc. Jpn.* **78**, 083701 (2009).

34. Paglione, J. & Greene, R. L. High-temperature superconductivity in iron-based materials. *Nat. Phys.* **6**, 645 (2010).

35. Sefat, A. S. Pressure effects on two superconducting iron-based families. *Rep. Prog. Phys.* **74**, 124502 (2011).

36. Okada, H. *et al*. Superconductivity under High Pressure in LaFeAsO. *J. Phys. Soc. Jpn.* **77**, 113712 (2008).

37. Takahashi, T. *et al*. High-pressure studies on superconductivity in LaFeAsO$_{1-x}$F$_x$ and SmFeAsO$_{1-x}$F$_x$. *J. Supercond. Nov. Magn.* **22**, 595 (2009).

38. Schilling, J., Hillier, N. & Foroozani, N. What have we learned from high-pressure experiments on Cu-oxide and Fe-based superconductors? *J. Phys.: Conf. Ser.* **449**, 012021 (2013).

39. Jin, K., Butch, N. P., Kirshenbaum, K., Paglione, J. & Greene, R. L. Link between spin fluctuations and electron pairing in copper oxide superconductors. *Nature* **476**, 73 (2011).

40. Lee, P., Nagaosa, N. & Wen, X. G. Doping a Mott insulator: Physics of high-temperature superconductivity. *Rev. Mod. Phys.* **78**, 1 (2006).

41. Sun, L. L. *et al*. Re-emerging superconductivity at 48 kelvin in iron chalcogenides. *Nature* **483**, 67 (2012).

42. Yin, Z. P., Haule, K. & Kotliar, G. Magnetism and charge dynamics in iron pnictides. *Nat. Phys.* **7**, 294–297 (2011).

43. Baek, S. –H. *et al*. NMR investigation of superconductivity and antiferromagnetism in CaFe$_2$As$_2$ under pressure. *Phys. Rev. Lett.* **102**, 227601 (2009).

44. Tinh, B. D. & Rosenstein, B. Theory of Nernst effect in high-Tc superconductors. *Phys. Rev. B* **79**, 024518 (2009).

45. Guo, J. *et al*. Pressure-driven quantum criticality in iron-selenide superconductors. *Phys. Rev. Lett.* **108**, 197001 (2012).

46. Ye, F. *et al*. High-pressure single-crystal neutron scattering study of magnetic and Fe vacancy orders in (Tl,Rb)$_2$Fe$_4$Se$_5$ superconductor. arXiv: 1405.4020.

47. Debessai, M., Matsuoka, T., Hamlin, J. J. & Schilling, J. S. Pressure-induced superconducting state of europium metal at low temperatures. *Phys. Rev. Lett.* **102**, 197002 (2009).

48. Mao, H. K., Xu, J. & Bell, P. M. Calibration of the ruby pressure gauge to 800 Kbar under quasi-hydrostatic conditions. *J. Geophys. Res.* **91**, 4673–4676 (1986).

49. Kresse, G. & Furthmüller, J. Efficient iterative schemes for ab initio total-energy calculations using a plane-wave basis set. *Phys. Rev. B* **54**, 11169 (1996).

50. Perdew, J. P., Burke, K. & Ernzerhof, M. Generalized gradient approximation made simple. *Phys. Rev. Lett.* **77**, 3865 (1996).

51. Blöchl, P. E. Projector augmented-wave method. *Phys. Rev. B* **50**, 17953 (1994).

Acknowledgments

Author contributions

D.G., J.G., P.G. and L.S. performed high-pressure resistance and *ac* susceptibility measurements. D.G., Y.Z., B.S. and A.S. grew the single crystals. D.G., S.Z., C.Z., L.X., R.L, Y.L. X.L. and J.L. carried out high-pressure X-ray diffraction measurements. D.G. and S.J. did refinements. X.D., C.L. and J.H. performed calculations. L.S., Q.W., D.G., A.S., J.H. and Z.Z. wrote the paper. All the authors analyzed the data and discussed the results.

Additional information